Organic Chemistry Plus
http://ojs.wiserpub.com/index.php/OCP/

UNIVERSAL WISER PUBLISHER

Research Article

Theoretical Study on Formamide (NH_2CHO) and Methylidene (CH_2) Reactions for the Formation of Interstellar *N*-Methylformamide

Shivani[1], Aftab Ahamad[1, 2], Manisha Singh[1, 2], Keshav Singh[1, 2], Alka Misra[1*], Poonam Tandon[2]

[1]Department of Mathematics & Astronomy, University of Lucknow, Lucknow, 226007, India
[2]Department of Physics, University of Lucknow, Lucknow 226007, India
E-mail: alkamisra99@gmail.com

Received: 10 March 2022; **Revised:** 28 April 2022; **Accepted:** 9 May 2022

Abstract: *N*-methylformamide (NMF), *E* & *Z* containing an amide bond, a vital component of peptides, is one of the simplest derivatives of formamides. It is detected towards the hot molecular core of the Sgr B2(N2) molecular cloud with the Atacama Large Millimeter/submillimeter Array (ALMA). It is proposed that the radical-molecule mechanism can be used as a strong contrivance to investigate the formation of NMF in the interstellar medium (ISM) via some interstellar molecules like methylidene CH_2 ($1_{\Sigma1}$ & $3_{\Sigma1}$) and formamide (NH_2CHO). The density functional theory (DFT) at B3LYP/6-311G (d,p) has been applied to study the mechanisms. All the possible cases of *E*- & *Z*-NMF formation with singlet and triplet CH_2 have been investigated. It is found that the formation of *E*-NMF with CH_2 ($1_{\Sigma1}$) and *Z*-NMF with CH_2 ($3_{\Sigma1}$) is more feasible and favorable in comparison to *E*-NMF formation from CH_2 ($3_{\Sigma1}$) and *Z*-NMF with CH_2 ($1_{\Sigma1}$).

***Keywords*:** astrobiology, ISM: molecules, ISM: clouds

1. Introduction

Amino acids are the fundamental building blocks of life-formation on earth and are linked together by amide bonds (-NHCHO-) to form proteins. Therefore, peptide bond-containing molecules play a pivotal role in the origin of life and have attracted special attention in terrestrial and prebiotic chemistry.[1] However, the detection of amino acids has not been confirmed in the interstellar medium (ISM)[2] but some molecules with peptide moiety have been detected in ISM *viz.* isocyanic acid (HNCO), formamide (NH_2CO), and acetamide (CH_3CONH_2). Tentative detection of interstellar *N*-methylformamide (NMF) has also been reported through rotational spectroscopy and chemical modelling.[3]

NMF (CH_3NHCHO) is also a molecule containing an amide bond, therefore, it may have biological importance in interstellar prebiotic chemistry. It is the simplest derivative of formamide and has a reasonable interest in interstellar detection because its structural isomer acetamide (CH_3CONH_2) has already been detected in ISM.[4,5] CH_3NHCHO is the second most stable isomer of C_2H_5NO after acetamide.[6] Belloche et al.[3] have reported the rotational spectra of *trans* conformer of NMF having 9,469 distinct line frequencies with $J \leq 62$ towards Sgr B2(N2). They also discussed chemical models for the formation of interstellar NMF towards Sgr B2(N2) and stated that CH_3NHCHO can be formed on grains either through the addition of functional-group radicals or *via* hydrogenation of methyl isocyanate (CH_3NCO).

In the present work, a radical reaction between NH_2CHO and CH_2 has been investigated for the formation of

DOI: https://doi.org/10.37256/ocp.3220221388

interstellar NMF. Both reactants used in this reaction path are well detected and abundant in ISM. Formamide (NH_2CHO) containing an amide bond manifests its key relevance towards prebiotic interstellar chemistry. It has been recognized as an interstellar moiety back in the early 1970s and has been detected in the gas-phase in ISM into Sgr B2 with column density $\leq 2.2 \times 10^{16}$ cm^{-2} and $\geq 4 \times 10^{11}$ cm^{-2}.[7] CH_2 is presumably abundant in primarily diffuse and dense clouds. The CH_2 abundance based on $N(H_2) \sim 3 \times 10^{23}$ cm^{-2} is on the order of 10^{15} - 10^{14} cm^{-2}. Hollis et al.[8] have, so far, made the only definite identification of CH_2 in the ISM, confirming their earlier detection.[9] CH_2 is detected in Orion-KL and W51 M molecular cloud through spectral line detection with column density 10^{15} and 10^{14} cm^{-2} respectively. It is detected in Sgr B2 and W49 N as well by far-infrared spectroscopy. The column density of CH_2 as observed is $(7.5 \pm 1.1) \times 10^{14}$ cm^{-2}.[8,10] In the proposed pathway, the reaction of NH_2CHO with both singlet and triplet CH_2 has been explored.

However, modeling the reactions for the formation of molecules and their precursors is a painstaking task and it is necessary to propose the reactions that occur at extremely low densities and temperatures. Computational chemistry provides a direct tool for understanding systems that are too complex to be observed experimentally. It is also used widely to interpret interstellar chemical reactions. Using quantum chemical techniques, the formation of NMF has been explored in a single-step reaction in the gas phase and icy grains. Many computational studies have been performed for the formation of biologically important molecules in ISM *viz*., glycolaldehyde, acetic acid, hydrogen cyanide, amino methanol, etc.[11-22]

2. Methodology

The calculations are performed with the help of Gaussian 09 software[23] at room temperature. The geometries of the different species involved in the reaction path have been optimized at the B3LYP/6-311G (d,p). Density functional theory, DFT/B3LYP is most widely used as it is computationally inexpensive and provides reliable and accurate results in comparison to other methods.[24] The optimized structure of each involved geometry is verified by vibrational analysis at the B3LYP/6-311G (d,p) level of theory. The stable geometries of reaction complex (RC) and product (P) have no imaginary frequencies while the transition state (TS) has a single imaginary frequency. Total energies (TE), zero-point vibrational energy (ZPVE), and electronic energies (EE) of all geometries formed during the reaction path toward the formation of NMF were calculated and are given in Table 1. An estimate of the rate coefficient is made based on equation (1):

$$k = 7.41 \times 10^{-10} \alpha^{1/2} (10/\mu)^{1/2} \text{ cm}^3 \text{ s}^{-1} \quad (1)$$

where α is the polarizability in $Å^3$ and μ is the reduced mass of the reactants on the ^{12}C amu scale.[25] Equation 1 is the Langevin formula for rate coefficients which is temperature independent. Frequency calculations give the value of standard enthalpies ΔH^o and Gibbs free energies ΔG^o of the compound under study. The thermodynamic equation $\Delta S^o = (\Delta H^o - \Delta G^o)/T$ is used to evaluate the entropy of the reaction ΔS^o (where T is temperature).

All reactions are studied both in the gas phase and IEF-PCM (Integral Equation Formalism-Polarizable Continuum Model).[26-30] Such PCM formulations investigate the effect of water icy grains on reactions, including the bulk solvation effect for which the dielectric constant Є = 78.5, is equal to that of liquid water.

3. Results and discussion

The dust grains act as a catalyst for the interstellar gas-phase reactions which lead to absorbing the heat released during the reactions. Gas-phase reactions mostly occur on surfaces of the dust grain. Two bodies can react with each other in the gas phase and can accrete at dust particles acting as the third body, which absorbs the heat of the reaction. The same role has been played by icy grains/cavities in icy grains reactions. The heat of the reaction is represented by infrared (IR) vibrations. We propose the following reaction path for the formation of NMF in the ISM.

3.1 *Reaction path*

$$CH_2(1_{\Sigma 1}\ \&\ 3_{\Sigma 1}) + NH_2CHO \rightarrow (E\ \&\ Z)\text{-}CH_3NHCHO \quad (2)$$

N-methylformamide exists both in *E* and *Z* forms and CH_2 exists in singlet $(1_{\Sigma 1})$ and triplet $(3_{\Sigma 1})$ states. All cases have been discussed in the gas phase and IEF-PCM.

3.1.1 *Mechanism 1*

$$CH_2(1_{\Sigma 1}) + NH_2CHO \rightarrow E\text{-}CH_3NHCHO \quad (3)$$

This reaction shows the radical molecule mechanism to form *E*-NMF in the ISM. Mulliken population analysis of reactants shows that atomic charges on C of $CH_2(1_{\Sigma 1})$ is -0.214 e.s.u., H atom of NH_2CHO are 0.226 e.s.u. (2H), 0.229 e.s.u. (3H) and 0.054 e.s.u. (6H), N atom of NH_2CHO is -0.420 e.s.u. and C atom of NH_2CHO is 0.258 e.s.u. These charges indicate the strong electrostatic attraction between the 7C atom of CH_2 and the 3H atom of NH_2CHO. Initially, the 3H-1N bond breaks, and the 3H atom gets attached to the 7C atom with a CH bond length of 1.094 Å. When the 3H atom is attached to 7C, then 1N (-0.443 e.s.u.) becomes more electronegative and forms a complex [CH_3---N(--H)HCO]. There is a strong attraction between 1N and 7C due to their electronegative and electropositive characters respectively. Further 1N atom reacts with 7C atom and is optimized at the bond length of 1.450 Å. The ground state geometry of *E*-NMF has been observed with the reaction of CH_2 and NH_2CHO having reaction energy -100.59 kcal mol^{-1} i.e., the reaction is exothermic. No TS has been found in this reaction mechanism. The rate coefficient of the reaction is calculated to be 1.5×10^{-9} cm^3 s^{-1} and also signifies the feasibility of the proposed reaction in the ISM. Thermochemistry parameters have been calculated to observe the feasibility of the reaction. The change in the calculated values of Gibbs free energy (ΔG^o), enthalpy (ΔH^o), and entropy (ΔS^o) of the above-mentioned reaction are -90.720 kcal mol^{-1}, -102.307 kcal mol^{-1}, and -38.883 cal mol^{-1} K^{-1} respectively. The spontaneity and exothermicity of the reaction are justified by the negative values of thermodynamic parameters, i.e. ΔG^o, ΔH^o, and ΔS^o at low temperatures. Hence, the reaction is thermodynamically feasible, spontaneous, and exothermic in the ISM also.

Similar calculations are also carried out in the PCM or icy grains cavity. CH_2 reacts with NH_2CHO in PCM and forms *E*-NMF with reaction energy -96.51 kcal mol^{-1}. Mulliken population analysis of molecules in PCM or icy grains shows that atomic charge on C (of CH_2) is -0.263 e.s.u., H of NH_2CHO is 0.243 e.s.u. (2H), 0.259 e.s.u. (3H), 0.080 e.s.u. (6H), N atom of NH_2CHO is -0.421 e.s.u. and C atom of NH_2CHO is 0.252 e.s.u. These atomic charges have a stronger electrostatic attraction in comparison to the gas phase. The reaction mechanism for the formation of *E*-NMF in PCM is similar to the reaction mechanism in the gas phase. The rate coefficient of the reaction in PCM or icy grains cavity is calculated to be 1.7×10^{-9} cm^3 s^{-1} which is higher than in the gas phase. The values of rate coefficient and reaction energy indicate that the reaction is more feasible and exothermic in the icy grains cavity or PCM in comparison to the gas phase.

According to ground state energy values (Table 1), it can be clearly stated that *E*-NMF formed under PCM calculations is more stable than gas-phase calculations. The thermodynamical parameters (ΔG^o, ΔH^o, and ΔS^o) are quite supportive of the spontaneity and feasibility of this reaction in ISM.

3.1.2 *Mechanism 2*

$$CH_2(1_{\Sigma 1}) + NH_2CHO \rightarrow Z\text{-}CH_3NHCHO \quad (4)$$

The *Z*-conformer of NMF can also be formed with the same reaction mechanism as mentioned above. This reaction involves the potential barrier. *Z*-NMF formation has been started with the formation of an RC with a distance of 2.19 Å between 7C & 3H. As discussed above the 3H atom gets attached to the 7C atom of CH_2 due to the strong electrostatic attraction force. Then, a TS [CH_3---NHCHO] has been obtained at the distance of 2.60 Å between 3C & 1N and angle 1N-7C-3H of 73.82°. The TS has a negative vibrational frequency of -645.97 cm^{-1} and a potential barrier of 3.70 kcal mol^{-1}, which is feasible in an ISM. The reaction is possible due to the quantum tunneling of the hydrogen atom. After crossing the potential barrier the *Z*-NMF has been formed with reaction energy -97.01 kcal mol^{-1}. The rate coefficient

of this reaction is calculated in the gas phase to be 1.6×10^{-9} cm^3 s^{-1}. The values of thermochemistry parameters such as ΔG^o, ΔH^o, and ΔS^o are found to be -90.79 kcal mol^{-1}, -102.31 kcal $mol^{-1,}$ and 101.71 cal mol^{-1} K^{-1} respectively. The negative values of ΔG^o, ΔH^o, and the positive value of ΔS^o show that the reaction is spontaneous and exothermic. Hence, the reaction is also thermodynamically feasible.

The TS between *E* & *Z* has also been obtained with the vibrational frequency -1892.19 cm^{-1}. The potential barrier of 105.68 kcal mol^{-1} has been observed which shows that the conversion of *E*-conformer to *Z*-conformer is not possible at room temperature. All the calculations are also carried out in the PCM or icy grains cavity with the same mechanism, as discussed above. After the formation of RC, the TS with a potential barrier of 4.94 kcal mol^{-1} has been observed. The negative vibration frequency of TS is obtained as -645.97 cm^{-1}. The increase in the potential barrier in PCM from the gas phase is attributed to the greater stabilization of the RC against that of a TS. This increase in the potential barrier is mainly due to the low activity of reactants in a polar solvent medium. After crossing the potential barrier, the *Z*-NMF has been formed with reaction energy -97.45 kcal mol^{-1}. The rate coefficient of the reaction is calculated at 1.9×10^{-9} cm^{-3} s^{-1} in the gas phase which shows the reaction is more feasible in PCM, in comparison to the gas phase. As discussed in the gas phase mechanism, the values of thermodynamical parameters {ΔG^o (-ve), ΔH^o (-ve), and ΔS^o (-ve)} also signify the spontaneity and exothermicity of the reaction in icy grains cavity or PCM (as explained in the gas phase). The lower value ground state energy (Table 1) of *Z*-NMF in PCM signifies that the product is more stable in the icy grains cavity in comparison to the gas phase.

All the involved optimized geometries for the formation of NMF have been shown in Figure 1 (for mechanisms 1 & 2).

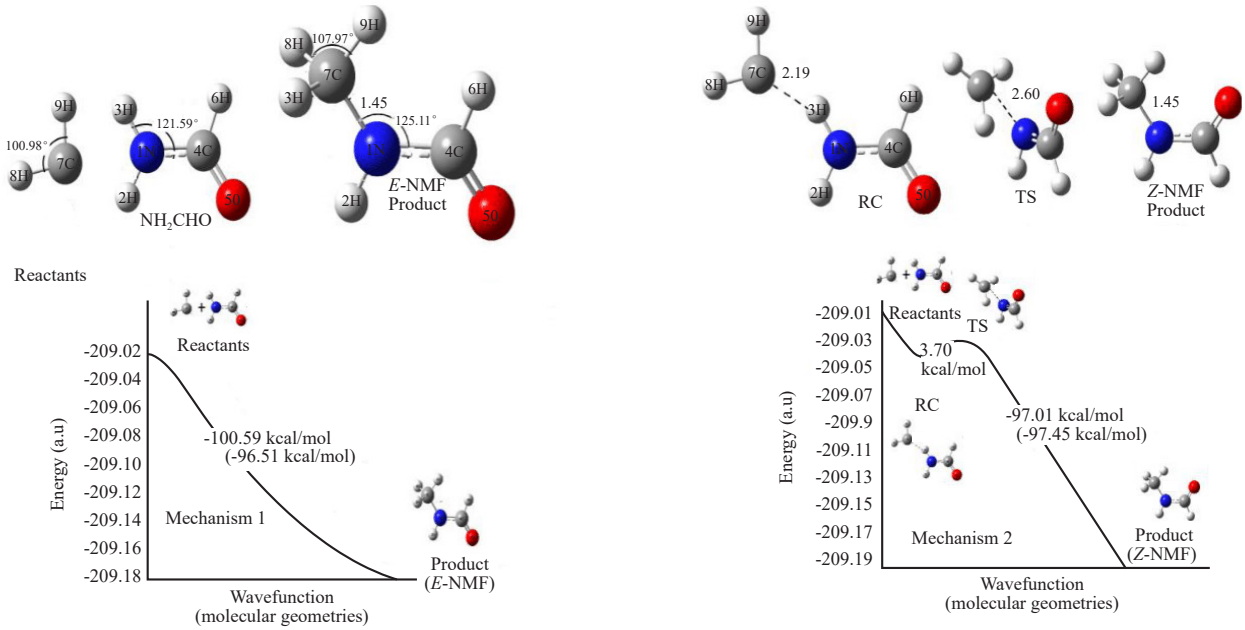

Figure 1. Optimized geometries and energy curves of mechanisms 1 & 2 for the formation of *E*- & *Z*-NMF with singlet CH_2. Bond lengths are in Å. Reaction energies in PCM and gas phase are given in parenthesis and without parenthesis respectively (shown in energy curves)

3.1.3 *Mechanism 3*

$$CH_2(3_{\Sigma 1}) + NH_2CHO \rightarrow E\text{-}CH_3NHCHO \quad (5)$$

In this reaction, the *E*-NMF has been formed through an RC and TS. When triplet CH_2 reacts with NH_2CHO molecule, an RC has been formed at 2.19 Å distance (between 7C & 3H) with the same values of Mulliken charges as

in the case of mechanism 1. In the next step, the quadratic synchronous transit 3 (QST3) has been applied to locate the TS. Due to the strong electrostatic attraction, the 3H atom gets attached to 7C and forms TS [CH_3---NHCHO], having a negative vibrational frequency of -672.18 cm^{-1}. The TS has been optimized at a distance of 2.80 Å (between 7C & 1N) and an angle 1N-7C-3H of 11.13°. The *E*-NMF has been formed after crossing the potential barrier of 14.79 kcal mol^{-1}. This barrier is high in comparison to previous mechanism 2. To form the required product, initially, 3H gets attached to 7C and forms CH_3-, a highly reactive free radical which makes 3C, highly prone to reacting site. 7C atom gets attracted towards the 1N atom and forms *E*-CH_3NHCHO with reaction energy -88.47 kcal mol^{-1}. The rate coefficient of the reaction is 1.6×10^{-9} cm^{-3} s^{-1} in the gas phase. The thermodynamical parameters have also been calculated to verify the feasibility of the reaction in the ISM. The values of ΔG^o, ΔH^o, and ΔS^o are found to be -78.19 kcal mol^{-1}, -90.12 kcal mol^{-1}, and -40.01 cal mol^{-1} K^{-1} respectively. Hence, the reaction is feasible in the ISM as thermodynamical parameters are supportive of the feasibility, spontaneity, and exothermicity of the reaction.

A similar mechanism has also been followed in PCM calculations. Initially, the formation of the RC takes place then, the TS has been found with a vibration frequency of -615.78 cm^{-1}. The potential barrier of 12.68 kcal mol^{-1} has been observed, which is comparatively less than the gas phase barrier. After penetrating the potential barrier, the required product *E*-NMF has been formed in icy grains having reaction energy -87.16 kcal mol^{-1}. The rate coefficient of this reaction is calculated in the gas phase to be 1.8×10^{-9} cm^{-3} s^{-1}. The negative values of the Gibbs free energy change (ΔG^o) & enthalpy change (ΔH^o) and positive value of entropy change (ΔS^o) show the thermodynamical feasibility, spontaneity, and exothermicity of the reaction in the ISM.

The reaction of triplet CH_2 with NH_2CHO acquires a positive activation barrier at the entrance channel i.e. in this mechanism, the energy of the TS lies above the total energy of reactants. The RC energy is also higher than the energy of reactants. Thus, it can be stated that this RC will be an intermediate that is obtained between TS and reactants. This reaction is feasible according to the calculations (rate coefficients and thermodynamical parameters) but due to the presence of an activation barrier it could to be tough also. Reactions having activation barriers need external energy sources to proceed with the reaction which may or may not be possible in a particular case.

3.1.4 *Mechanism 4*

$$CH_2(3_{\Sigma 1}) + NH_2CHO \rightarrow Z\text{-}CH_3NHCHO \quad (6)$$

It is an exothermic and barrierless reaction. The Mulliken charge analysis of CH_2 shows the charge on the C atom is -0.281 e.s.u. and charges of NH_2CHO atoms are similar as in the case of mechanism 1. The reaction initiates with the electrostatic attraction between the 2H atom of NH_2CHO towards the 7C atom of CH_2. So, the 2H atom detached from the 1N atom (-0.386 e.s.u.), and a 7C-1N bond has been formed first due to the presence of lone pair on 7C and free-electron on the 1N atom and also because of their electropositive and electronegative character respectively. After the formation of a 7C-1N bond, an electron on a 7C atom remains unpaired so it gets bonded with the 2H atom that has an unpaired electron. Hence, a final product, *Z*-NMF, has been formed having a reaction energy of -89.48 kcal mol^{-1}. The rate coefficient of this reaction is calculated in the gas phase to be 1.6×10^{-9} cm^{-3} s^{-1}. The thermodynamical parameters (ΔG^o, ΔH^o, and ΔS^o) have also been calculated to verify the feasibility of the reaction in the ISM and are found to be -79.36 kcal mol^{-1}, -91.21 kcal mol^{-1}, and -39.75 cal mol^{-1} K^{-1} respectively, which are supportive for the feasibility, spontaneity, and exothermicity of reaction in the ISM.

A similar mechanism has been followed in the icy grains or PCM model. The product has been formed with the reaction of CH_2 and NH_2CHO with reaction energy -88.10 kcal mol^{-1}. The reaction is exothermic and barrierless. The rate coefficient of this reaction is calculated in the gas phase to be 1.7×10^{-9} cm^{-3} s^{-1}. The negative values of ΔG^o, ΔH^o, and ΔS^o signify the thermodynamical feasibility, exothermicity, and spontaneity of the reaction in the ISM.

All the involved optimized geometries and energy curves have been shown in Figure 2 (mechanisms 3 & 4) for the formation of NMF. All the energies *viz.*, EE, ZPVE, and TE for all the above-mentioned mechanisms are calculated and tabulated in Table 1.

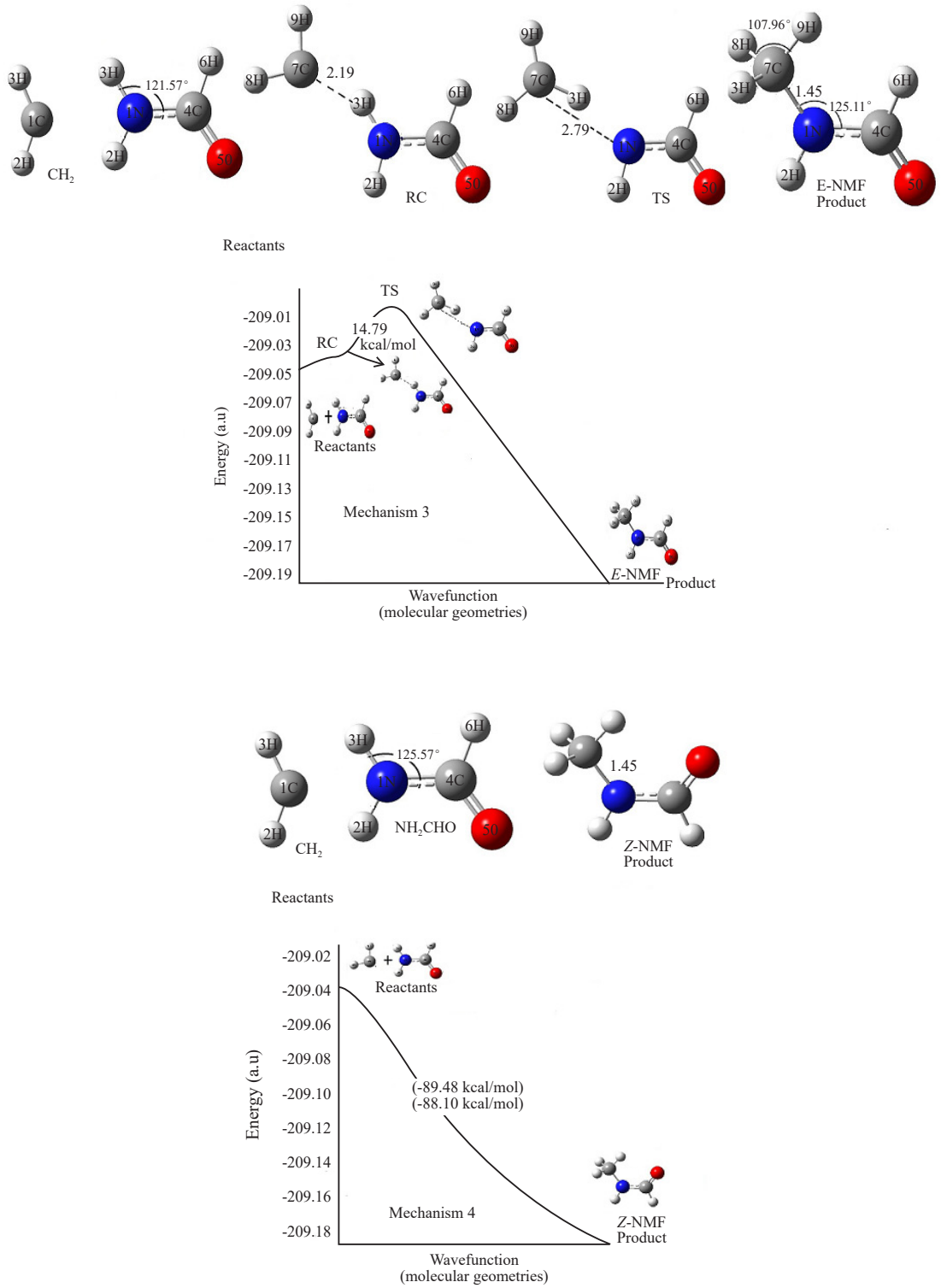

Figure 2. Optimized geometries and energy curves of mechanisms 3 & 4 for the formation of *E*- & *Z*-NMF with triplet CH_2. Bond lengths are in Å. Reaction energies in PCM and gas phase are given in parenthesis and without parenthesis respectively (shown in energy curves).

Table 1. Calculated EE, ZPVE, and TE of all involved geometries in the formation of *E*- & *Z*-conformers of NMF from singlet and triplet states of CH_2 with B3LYP/6-311G (d,p)

	CH_2 Singlet: NMF					
	Gas Phase			PCM		
	EE	ZPVE	TE	EE	ZPVE	TE
CH_2	-39.1444	0.0165	-39.1279	-39.1501	0.0165	-39.1336
NH_2CHO	-169.9463	0.0453	-169.9010	-169.9566	0.0453	-169.9113
E-CH_3NHCHO (*E*-NMF)	-209.2631	0.0739	-209.1892	-209.2725	0.0738	-209.1987
RC (*Z*)	-209.1011	0.0647	-209.0364	-209.1138	0.0647	-209.0491
TS (*Z*)	-209.0986	0.0681	-209.0305	-209.1101	0.0684	-209.0417
Z-CH_3NHCHO (*Z*-NMF)	-209.2650	0.0740	-209.1910	-209.2743	0.0740	-209.2002
	CH_2 Triplet: NMF					
	Gas Phase			PCM		
	EE	ZPVE	TE	EE	ZPVE	TE
CH_2	-39.1645	0.0172	-39.1473	-39.1656	0.0172	-39.1485
NH_2CHO	-169.9463	0.0453	-169.9010	-169.9566	0.0453	-169.9113
RC (*E*)	-209.1011	0.0647	-209.0364	-209.1146	0.0646	-209.0500
TS (*E*)	-209.0787	0.0643	-209.0144	-209.0940	0.0643	-209.0298
E-CH_3NHCHO (*E*-NMF)	-209.2631	0.0739	-209.1892	-209.2725	0.0738	-209.1987
Z-CH_3NHCHO (*Z*-NMF)	-209.2650	0.0740	-209.1909	-209.2743	0.0740	-209.2002

3.2 *Vibrational analysis*

The theoretical and experimental IR spectrum of NMF has good agreement as shown in Figure 3. The theoretical spectrum is obtained from Gaussian calculations and the experimental spectrum has been taken from the National Institute of Standards and Technology (NIST) Chemistry WebBook, SRD 69 [https://webbook.nist.gov/cgi/cbook.cgi?ID=C123397&Mask=80#].[31]

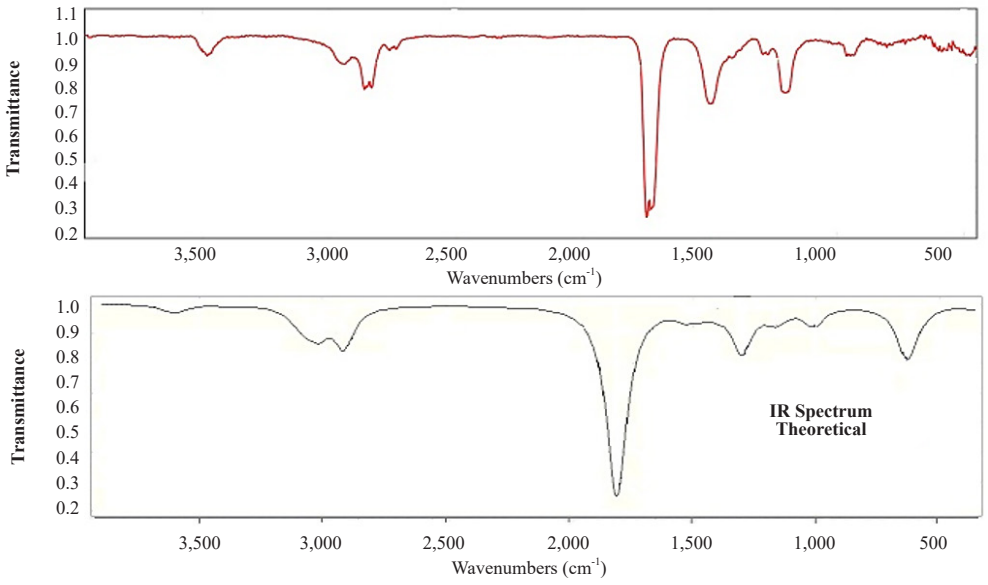

Figure 3. Comparison between experimental and theoretical IR spectrum of NMF

The optimized geometry of NMF through DFT has an accurate agreement with experimentally observed geometry. DFT is an authoritative technique to explain gas-phase geometries and dynamical changes by deriving DFT-configured force fields completely. The geometrical analysis of *E*- & *Z*-NMF derived from DFT calculations with B3LYP/6-311G (d,p) basis sets is presented in Table 2 and compared with the experimentally observed vibrations of NMF from gas-phase electron diffraction studies reported by Mitsuo and Kozo.[32] The simple vibrational analysis provides useful information regarding the arrangement of atoms and structure in space. The wavenumber linear scaling procedure (WLS) has been used to scale down the wavenumbers.[33] The scaled wavenumbers obtained at B3LYP/6-311G (d,p) basis set have good agreement with the experiment data. The theoretical scaled and experimental wavenumbers for NMF are given in Table 3. The experimental and calculated IR spectrum is given in Figure 3. The N-H stretching absorption generally occurred in the region 3,500-3,220 cm^{-1}.[34] In the experimental FT-IR (Fourier transform infrared spectroscopy) spectra of NMF, the N-H stretching vibration is observed at 3,465 cm^{-1} whereas calculated at 3,455 cm^{-1} FT-IR spectra. The fundamental modes involved in NH vibrations are asymmetric stretching, symmetric stretching, and bending vibrations. The symmetric stretching of N-H is calculated at 3,455 cm^{-1} and correlates well with the observed experimental wavenumber at 3,465 cm^{-1}. The experimental C-H in-plane bending vibrations are obtained in the 1,300-1,000 cm^{-1} region[34] and calculated C-H bending modes are found in the range of 1,350-1,470 cm^{-1}. The corresponding bands are observed in the experimental spectrum at 1,390 cm^{-1} and 1,290 cm^{-1}. The percentage of contributions of these vibrations towards other frequencies is given in Table 3. The out-of-plane C-H deformation modes are predicted to occur in the region 1,000-600 cm^{-1}. The oop (out-of-plane) C-H deformation and torsion modes are clearly defined in Table 3. In general, C=O stretching vibrations in the region of 1,870-1,540 cm^{-1} give rise to an absorption band. The C=O stretching bands were observed at 1,695 cm^{-1} in the spectrum. This absorption peak is calculated to be at 1,734 cm^{-1} at B3LYP/6-311G (d,p) basis set and the corresponding peak in experimental spectra is at 1,695 cm^{-1} which corresponds well with the calculated values.

Table 2. Bond lengths and bond angles of *E*- & *Z*-NMF by using B3LYP/6-311G (d,p)

	Bond Lengths (Å)					
	C7H8	C7H3	C7H2	N1C7	N1H2	N1H3
E-CH_3NHCHO(*E*-NMF)	1.09429	1.09437	---	1.45044	1.011	---
Z-CH_3NHCHO(*Z*-NMF)	1.09378	---	1.08866	1.45422	---	1.00768
	Bond Angles (degrees)					
	H8C7H9	C4N1C7	N1C4O5		C4N1H2	C4N1H3
E-CH_3NHCHO(*E*-NMF)	107.96583	125.11743	125.20469		115.60740	133.80761
Z-CH_3NHCHO(*Z*-NMF)	108.9636	122.88228	125.57592		92.58976	117.86057

Table 3. Experimental and calculated infrared spectra of *E*-NMF. Frequencies in cm^{-1}

Modes	Experimental Wave No.	Calculated Scaled Wave No.	PED (Potential Energy Distribution) Contributions Cord (% > = 5%)
21	3465	3455	ν(NH)(100)
20	2890	2984	ν_{ays}(C7H3 + C7H8)(86) + ν_{ays}(C7H2)(14)
19	2940	2945	ν(C7H8)(51) + ν(C7H3)(49)
18	2844	2896	ν_{sym}(C7H3)(100)
17	2754	2796	ν(C4H6)(99)
16	1695	1734	ν(C4O)(71) - ν(NC4)(11) + ρ(C4H6)(10) + ω(N1H2)(8)
15		1473	δ_{ays}(CH3)(61) + ρ(CNH)(22)
14		1427	δ'_{ays}(CH3)(37) + ρ(CNH)(20) + δ_{ays}(CH3)(15) + ρ(HC4O)(7)
13		1427	δ_{ays}(CH3)(54.) + ρ(CNH)(14) + δ_{ays}(CH3)(10)
12	1390	1409	δs(CH3)(88)
11		1341	ρ(HC4O)(75) + t(CH3)(13)
10	1290	1246	ω(NH)(47) + (CH3)(23) + δ_{sci}(OC4N)(11)
9		1114	ν(NC7)(50) + ρ(C7HN)(24) + ρ(C7HN)(8) + δ_{sci}(C7C4N)(6)
8		1102	ρ(C7HN)(69) + ρ(C7HN)(23) + δ'_{ays}(CH3)(7)
7		1001	δ_{out}(NC4O)(92) + t(C4N)(7)
6		968	ρ(C7HN)(26) + ν(NC7)(23) + ν(NC4)(14) + δ_{sci}(OC4N)(12) + ω(NH)(11) + ρ(C7HN)(9)
5		606	τ(C4N)(57) + ρ(CH3)(37)
4		586	δ_{sci}(OC4N)(50) + ν(NC7)(19) + ν(NC4)(13) + δ_{sci}(C7C4N)(9)

Types of vibrations: ν - stretching, δ_{sci} - scissoring, ρ - rocking, ω - wagging, δ - deformation, t - torsion.

3.3 *Global and local descriptors*

The local and global electronic descriptors have been calculated by using various standard methods.[35-39] These descriptors are derived from B3LYP/6-311G (d,p) and are shown in Table 4. Global reactivity descriptors such as electronegativity (χ), chemical potential (μ), global hardness (η), global softness (S), and electrophilicity index (ω) are highly recommended in predicting global reactivity trends. The following equations are used to calculate, such as: $\chi = -1/2(\varepsilon_{LUMO} + \varepsilon_{HOMO})$; $\mu = 1/2\ (\varepsilon_{LUMO} + \varepsilon_{HOMO})$; $\eta = 1/2\ (\varepsilon_{LUMO} - \varepsilon_{HOMO})$; $S = 1/2\eta$; $\omega = \mu^2/2\eta$. The local reactivity descriptors such as Fukui functions $f_k^+(r), f_k^-(r), f_k^0(r)$ can be given as: $f_k^+(r) = [q_k(N+1) - q_k(N)]$, for nucleophilic attack; $f_k^-(r) = [q_k(N) - q_k(N-1)]$, for electrophilic attack; $f_k^0(r) = 1/2[q_k(N+1) + q_k(N-1)]$, for radical attack, where, ρ is the electron density of atom k in the molecule, q is the gross charge of atom k in the molecule and N, N+1, N-1 are electron systems containing neutral, anion, cation form of molecule, respectively.[35,37,40-42] The neutral, cation, and anion state of the molecule has been analyzed via the Hirschfield population. The selection of reacting site of the molecule has been confirmed through Fukui functions (Table 4).

Table 4. Calculated global and local reactivity descriptors (eV)

Molecules/Atoms	Global Descriptors				Local Descriptors			
	η	S	μ	ω	f_k^0	n_k^0	s_k^0	ω_k^0
CH_2	**1.6439**	**0.8220**	**-5.2715**	**3.3576**				
C					0.6217	1.0220	0.5110	2.0874
H					0.1891	0.3109	0.1554	0.6349
H					0.1891	0.3109	0.1554	0.6349
NH_2CHO	**3.8571**	**1.9285**	**-3.2867**	**3.0624**				
1N					0.0483	0.1863	0.0931	0.1479

Table 4. *(Continued)*

2H					0.2231	0.8605	0.4302	0.6832
3H					0.3897	1.5031	0.7515	1.1934
4C					-0.0042	-0.0162	-0.0081	-0.0129
5O					0.1948	0.7514	0.3757	0.5966
6H					0.1483	0.5720	0.2859	0.4542
E-CH_3NHCHO	**3.8410**	**1.9205**	**-3.1895**	**2.8719**				
1N					0.0821	0.3153	0.1577	0.2358
2H					0.1520	0.5838	0.2919	0.4365
3H					0.2630	1.0101	0.5051	0.7553
4C					0.0433	0.1663	0.0832	0.1244
5O					0.1740	0.6683	0.3341	0.4997
6H					0.0986	0.3787	0.1893	0.2832
7C					-0.1816	-0.6975	-0.3488	-0.5215
8H					0.2241	0.8608	0.4304	0.6436
9H					0.1446	0.5554	0.2777	0.4153
RC (*Z*-CH_3NHCHO)	**1.0055**	**0.50275**	**-5.5309**	**0.5652**				
1N					0.0234	0.0235	0.0118	0.0132
2H					0.0610	0.0613	0.0307	0.0345
3H					0.0332	0.0334	0.0167	0.0188
4C					0.0565	0.0568	0.0284	0.0319
5O					0.1944	0.1955	0.0977	0.1099
6H					0.0803	0.0807	0.0404	0.0454
7C					0.3122	0.3139	0.1569	0.1765
8H					0.1220	0.1227	0.0613	0.0689
9H					0.1171	0.1177	0.0589	0.0662
TS (*Z*-CH_3NHCHO)	**1.2798**	**0.6399**	**-5.4730**	**2.8176**				
1N					0.1031	0.1319	0.0659	0.2905
2H					0.0584	0.0747	0.0374	0.1646
3H					0.0906	0.1159	0.0579	0.2553
4C					0.0412	0.0527	0.0264	0.1161
5O					0.1890	0.2419	0.1209	0.5325
6H					0.1577	0.2018	0.1009	0.4443
7C					0.1680	0.2150	0.1075	0.4734
8H					0.1220	0.1561	0.0781	0.3438
9H					0.0699	0.0895	0.0447	0.1969
Z-CH_3NHCHO	**3.8594**	**1.9297**	**-3.1989**	**0.7257**				
1N					0.0579	0.2235	0.1117	0.0420
2H					0.0600	0.2316	0.1158	0.0435
3H					0.3092	1.1933	0.5967	0.2244
4C					-0.0167	-0.0644	-0.0322	-0.0121
5O					0.1631	0.6294	0.3147	0.1184
6H					0.1769	0.6827	0.3414	0.1284
7C					-0.1095	-0.4226	-0.2113	-0.0795
8H					0.1796	0.6931	0.3466	0.1303
9H					0.1795	0.6928	0.3464	0.1303

The value of the Fukui function for the carbon atom of CH_2 is highest than its hydrogen atoms. Similarly, the 3H atom of NH_2CHO is the highest value of Fukui function in comparison to its other atoms. So, these hydrogen and carbon atoms are more prone to react or the most favorable reacting site. Hence, the nitrogen atom reacts with the carbon atom

of CH_2 and forms the *E*- & *Z*-CH_3NHCHO.

The energy transfer value (ECT) shows the charge flow direction from one to another reactant. ECT is calculated by the equation ECT = $(\Delta N_{max})_A$ - $(\Delta N_{max})_B$. ECT = 2.35 eV, which is > 0 implies that charge flows from NH_2CHO to CH_2. Therefore, CH_2 acts as an electron acceptor and NH_2CHO as an electron donor. The higher value of global publicity and lower value of chemical potential shows that CH_2 is a strong electrophile. Similarly, a lower value of global publicity and a higher value of chemical potential for NH_2CHO favor its nucleophilic behavior.

3.4 *Anharmonic calculations*

Density functional theory gives authentic information on anharmonic vibrational spectroscopic constants. DFT predictions are not as highly accurate as configuration integration (CI) methods but as good or better than coupled-cluster single double (CCSD) results and are often comparable with coupled-cluster single double (triplet) [CCSD (T)]. B3LYP performs the best of the DFT methods considered.[43] The centrifugal distortional constants have also been calculated at B3LYP/6-311G (d,p). Due to overall rotations and vibrations, atoms of a molecule get displaced from their average positions away from the center of gravity of the molecule. The quartic centrifugal distortion constants are based on Kivelson-Wilson formalism[44] for *E*- & *Z*-NMF and are shown in Table 5. A_e, B_e, C_e, and A_0, B_0, C_0 are the rotational constants corresponding to the equilibrium geometry and the ground state rotational constants of the molecule respectively. The rotational vibrational coupling constant (α) is calculated by using second-order perturbation theory which is obtained by:

$$\alpha = B_0 - B_1 \tag{7}$$

i.e. the difference between the ground state rotation constant (B_0) to the first excited state rotational constant (B_1).[45] The calculated rotational vibrational coupling constant for the *E*- & *Z*-conformer of NMF has been shown in Table 6.

Table 5. Rotational constants (cm^{-1}) including terms due to quadratic centrifugal distortion constants and Nielsen's and Wilson's centrifugal distortion constants ($\times 10^{-6}$ cm^{-1}) of NMF using B3LYP/6-311G (d,p)

Rotational Constants			Nielsen's Constants			Wilson's Constants	
	Z-	*E*-		*Z*-	*E*-	*Z*-	*E*-
A_e	0.6658831	1.4963851	D_J	0.142465	0.027505	0.0597818	0.021546
B_e	0.2034523	0.1453000	D_{JK}	-0.478822	0.101834	0.150089	0.0185851
C_e	0.1605810	0.1358409	D_K	2.43824	8.641693	0.0203715	-0.0088912
A_0	0.6585927	1.4714422	R5	0.122261	0.072630		
B_0	0.2027455	0.1445120	$\|R6\| \times 10^{-6}$	-0.00127322	0.000556		
C_0	0.1597118	0.1351139	$\Delta J \times 10^{-6}$	0.0426152	0.002423		

Value of D_J (*E*-NMF) < D_J (*Z*-NMF) shows that the stretching of bonds in *E*-NMF is less in comparison to *Z*-NMF due to centrifugal distortion force indicates that *E*-conformer is more stable than *Z*-conformer. The small magnitudes of distortion constants represent the optimized geometry has the least deformation from its equilibrium stable geometry due to rotations and vibrations.

Table 6. Rotational-vibrational coupling constants of (cm^{-1}) at B3LYP/6-311G (d,p)

	Z-NMF			*E*-NMF		
	a	b	c	a	b	c
α_1	0.00037	0.00036	0.00023	0.00223	0.00014	0.00014
α_2	0.00004	0.00020	0.00010	0.00326	-0.00003	-0.00001
α_3	0.00044	0.00012	0.00003	0.00201	-0.00004	-0.00003
α_4	0.00006	0.00015	0.00003	0.00344	0.00001	-0.00001
α_5	0.00056	0.00048	0.00025	0.00419	-0.00002	0.00001
α_6	0.00344	0.00003	0.00017	0.00172	0.00043	0.00039
α_7	0.00131	0.00004	0.00009	-0.01207	0.00008	-0.00021
α_8	0.01498	0.00052	0.00002	0.00434	-0.00144	-0.00004
α_9	0.01078	0.00015	0.00043	0.00152	0.00010	-0.00014
α_{10}	0.00482	0.00051	0.00057	0.01014	0.00151	0.00066
α_{11}	0.00071	0.00056	0.00008	-0.00078	-0.00015	0.00009
α_{12}	0.00226	0.00025	0.00007	0.00034	0.00021	0.00021
α_{13}	0.01366	0.00061	0.00044	-0.06266	0.00016	0.00049
α_{14}	0.01636	0.00087	0.00015	0.06570	0.00040	0.00015
α_{15}	0.00142	0.00031	0.00002	-0.00007	0.00018	-0.00002
α_{16}	0.00024	0.00091	0.00066	0.00459	0.00028	0.00031
α_{17}	0.00170	0.00013	0.00024	-0.00246	-0.00016	-0.00015
α_{18}	0.00335	0.00024	0.00024	0.01149	0.00017	0.00016
α_{19}	0.00733	0.00026	0.00058	-0.03929	0.00001	0.00015
α_{20}	0.00431	0.00032	0.00039	0.02249	0.00004	-0.00018
α_{21}	0.00386	0.00111	0.00060	0.02975	-0.00031	-0.00050

Table 7. Comparison of some distortion parameters

Distortion Constants	Theoretical Values[a]	Experimental Values[b]
Φ_J	0.2275×10^{-14}	0.4542×10^{-12}
Φ_K	0.5361×10^{-9}	0.2619×10^{-10}
Φ_{KJ}	-0.4650×10^{-9}	0.3394×10^{-10}
φ_j	0.1584×10^{-14}	0.2336×10^{-12}
φ_k	-0.2806×10^{-9}	0.2255×10^{-10}
φ_{jk}	-0.3653×10^{-11}	-0.6207×10^{-12}
Δ_J	0.2639×10^{-7}	0.3007×10^{-6}
Δ_{JK}	0.1085×10^{-6}	-0.8333×10^{-6}
Δ_K	0.8636×10^{-5}	0.3021×10^{-5}
δ_J	0.2423×10^{-8}	0.1082×10^{-6}
δ_K	-0.7824×10^{-6}	0.3674×10^{-6}

[a] Calculated values via B3LYP/6-311G (d,p)
[b] Values reported by Belloche et al.[3]

As it is clear from the table, most of the theoretical parameters have small values in comparison to experimentally calculated parameters. Hence, less deformation (sextic and quartic) has been found in our calculations. The new vibrational-rotational values may be helpful to study such molecules.

4. Conclusion

Based on DFT calculations performed through B3LYP/6-311G (d,p), the reaction mechanism to the *E*- & *Z*-NMF formation through singlet and triplet CH_2 is found to be barrierless and exothermic respectively, while the barrier is found vice-versa i.e., *E* & *Z* isomers. It reveals to be more pertinent in ISM than the process has known mechanisms so far. Mechanisms 1 and 4 are highly feasible in ISM as they are barrierless reactions. Mechanism 2 has a penetrable barrier so it is also feasible in ISM. The reaction of triplet CH_2 with NH_2CHO (mechanism 3) acquires the positive activation barrier due to which it is found to be inefficient in comparison to other discussed cases. It concludes that the small magnitude of distortion constants manifest that the optimized geometries have less deformation from their equilibrium state.

Relevance of Study:

- *Such kind of theoretical study provides an experimental chemical model to study the possibilities of the formation of biologically important interstellar molecules.*
- *This study confirms that the radical reaction of NH_2CHO and CH_2 is a feasible chemical mechanism with no potential barrier or small potential barrier to form NMF which has a great biological interest.*
- *A theoretical approach to studying the formation of NMF in ISM confirms the possibility of the carbon-containing extra-terrestrial life.*
- *As NMF is a structural isomer of acetamide with peptide bond and has great relevance in the formation of life.*
- *This type of research is multidisciplinary and motivates researchers to find the interstellar chemistry responsible for the formation of molecules in the ISM.*

Acknowledgement

The financial support to Alka Misra (PI) and Shivani (RA) from a major research project under the Centre of Excellence (COE) is gratefully acknowledged.

Conflict of interest

The authors declare that there is no conflict of interest.

References

[1] Kaiser, R. I.; Stockton, A. M.; Kim, Y. S.; Jensen, E. C.; Mathies, R. A. *Astrophys. J.* **2013**, *765* (2), 111-119.
[2] Sugahara, H.; Takano, Y.; Tachibana, S.; Sugawara, I.; Chikaraishi, Y.; Ogawa, N. O.; Ohkouchi, N.; Kouchi, A.; Yurimoto, H. *Geochem. J.* **2019**, *53* (1), 5-20.
[3] Belloche, A.; Meshcheryakov, A. A.; Garrod, R. T.; Ilyushin, V. V.; Alekseev E. A.; Motiyenko, R. A.; Margulès, L.; Müller, H. S. P.; Menten, K. M. *Astron. Astrophys.* **2017**, *601*, A49.
[4] Halfen, D. T.; Ilyushin, V.; Ziurys, L. M. *Astrophys. J.* **2011**, *743* (1), 60-72.
[5] Hollis, J. M.; Lovas, F. J.; Remijan, A. J.; Jewell, P. R.; Ilyushin, V. V.; Kleiner, I. *Astrophys. J.* **2006**, *643* (1), L25-L28.
[6] Lattelais, M.; Pauzat, F.; Ellinger, Y.; Ceccarelli, C. *Astron. Astrophys.* **2010**, *519*, A30-A36.
[7] Rubin, R. H.; Swenson, G. W. Jr.; Benson R. C.; Tigelaar, H. L., Flygare, W. H. *Astrophys. J.* **1971**, *169*, L39-L44.
[8] Hollis, J. M.; Jewell, P. R.; Lovas, F. J. *Astrophys. J.* **1995**, *438*, 259-264.
[9] Hollis, J. M.; Jewell P. R.; Lovas, F. J. *Astrophys. J.* **1989**, *346*, 794-798.
[10] Polehampton, E. T., Menten, K. M.; Brünken, S.; Winnewisser, G.; Baluteau, J. -P. *Astron. Astrophys.* **2005**, *431* (1), 203-213.
[11] Singh, A.; Misra, A.; Tandon, P. *Res. Astron. Astrophys.* **2013**, *13* (8), 912-920.
[12] Singh, A.; Shivani; Misra, A.; Tandon, P. *Res. Astron. Astrophys.* **2014**, *14* (3), 275-284.
[13] Shivani; Misra, A.; Tandon, P. *Origins Life Evol. Biospheres* **2014**, *44*, 143-157.

[14] Shivani; Singh, A.; Misra, A.; Tandon, P. *Astron. Astrophys.* **2014**, *563*, A55.
[15] Yadav, M.; Shivani; Misra, A.; Tandon, P. *Origins Life Evol. Biospheres* **2019**, *49*, 89-103.
[16] Ahmad, A.; Shivani; Misra, A.; Tandon, P. *Res. Astron. Astrophys.* **2020**, *20*, 14.
[17] Singh, K. K.; Shivani; Tandon, P. Misra, A. *Astrophys. Space Sci.* **2018**, *363*, 213.
[18] Singh, K. K.; Tandon, P. Misra, A.; Shivani; Yadav, M.; Ahmad, A. *Int. J. Astrobiol.* **2021**, *20* (1), 62-72.
[19] Singh, K. K.; Tandon, P. Misra, A.; Shivani; Yadav, M.; Ahmad, A.; Chaudhary, M. K. *Mon. Not. R. Astron. Soc.* **2021**, *506* (2), 2059-2065.
[20] Yadav, M.; Shivani; Ahamad, A.; Singh, K. K.; Singh, R.; Misra, A.; Tandon, P. *J. Mol. Struct.* **2022**, *1248*, 131460.
[21] Shivani; Pandey, P.; Misra, A.; Tandon, P. *Eur. Phys. J. D.* **2017**, *71*, 215.
[22] Shivani; Misra, A.; Tandon, P. *Res. Astron. Astrophys.* **2017**, *17* (1), 1-10.
[23] Frisch, M. J.; Trucks, G. W.; Schlegel, H. B.; Scuseria, G. E.; Robb, M. A.; Cheeseman, J. R.; Scalmani, G.; Barone, V.; Mennucci, B.; Petersson, G. A.; et al. *Gaussian 09*, Revision E.01; Gaussian, Inc.: Wallingford, CT, 2009.
[24] Scott, A. P.; Radom, L. *J. Phys. Chem.* **1996**, *100* (41), 16502-16513.
[25] Bates, D. R. *Astrophys. J.* **1983**, *270*, 564-577.
[26] Miertuš, S.; Scrocco, E.; Tomasi, J. *Chem. Phys.* **1981**, *55* (1), 117-129.
[27] Cancès, E.; Mennucci, B.; Tomasi, J. *J. Chem. Phys.* **1997**, *107*, 3032-3041.
[28] Mennucci, B.; Tomasi, J. *J. Chem. Phys.* **1997**, *106*, 5151-5158.
[29] Mennucci, B.; Cancès, E.; Tomasi, J. *J. Phys. Chem. B* **1997**, *101* (49), 10506-10517.
[30] Tomasi, J.; Mennucci, B.; Cancès. E. *J. Mol. Struct.: THEOCHEM* **1999**, *464* (1-3), 211-226.
[31] Wallace, W. E. Infrared Spectra. In *NIST Chemistry WebBook*, NIST Standard Reference Database Number 69; Linstrom, P. J., Mallard, W. G., Eds.; National Institute of Standards and Technology: Gaithersburg, MD, 2009. DOI: 10.18434/T4D303
[32] Mitsuo, K.; Kozo, K. *Bull. Chem. Soc. Jpn.* **1974**, *47* (3), 631-634.
[33] Yoshida, H.; Ehara, A.; Matsuura, H. *Chem. Phys. Lett.* **2000**, *325* (4), 477-483.
[34] Silverstein, R. M.; Webster, F. X.; Kiemle, D. J.; Bryce, D. L. *Spectrometric Identification of Organic Compounds*, 8th ed.; Wiley: New Jersey, 2014.
[35] Parr, R. G.; von Szentpály, L.; Liu, S. *J. Am. Chem. Soc.* **1999**, *121* (9), 1922-1924.
[36] Chattaraj, P. K.; Sarkar, U.; Roy, D. R. *Chem. Rev.* **2006**, *106* (6), 2065-2091.
[37] Parr, R. G.; Weitao, Y. Chemical Potential Derivatives. In *Density-Functional Theory of Atoms and Molecules*; Qxford Science Publication: New York, 1989; pp 87-101.
[38] Berkowitz, M.; Ghosh, S. K.; Parr, R. G. *J. Am. Chem. Soc.* **1985**, *107* (24), 6811-6814.
[39] Nalewajski, R. F.; Korchowiec, J.; Zhou, Z. *Int. J. Quantum Chem.* **1988**, *34* (S22), 349-366.
[40] Parr, R. G.; Pearson, R. G. *J. Am. Chem. Soc.* **1983**, *105* (26), 7512-7516.
[41] Geerlings, P.; De Proft, F.; Langenaeker, W. *Chem. Rev.* **2003**, *103* (5), 1793-1874.
[42] Chattaraj, P. K.; Giri, S. *J. Phys. Chem. A* **2007**, *111* (43), 11116-11121.
[43] Sinnokrot, M. O.; Sherrill, C. D. *J. Chem. Phys.* **2001**, *115* (6), 2439-2448.
[44] Kivelson, D.; Wilson, E. B. Jr. *J. Chem. Phys.* **1952**, *20* (10), 1575-1579.
[45] Barone, V. *J. Chem. Phys.* **2005**, *122* (1), 014108-1-014108-10.

Appendix

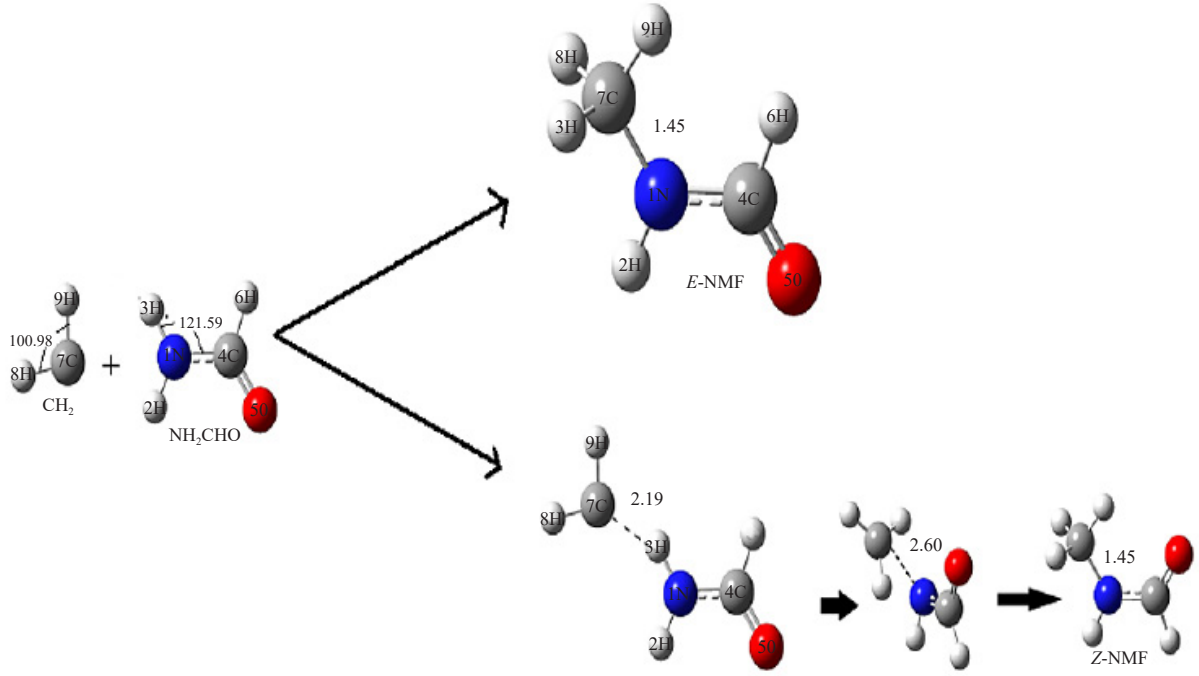

Figure A. Formation of *N*-methylformamide through interstellar molecules